

# Power law pseudo phase-space density profiles of dark matter halos: fluke of physics?

**Arpit Arora and Liliya L. R. Williams**

School of Physics and Astronomy, University of Minnesota,  
116 Church Street SE, Minneapolis, MN 55455, USA

E-mail: [arora125@umn.edu](mailto:arora125@umn.edu), [llrw@umn.edu](mailto:llrw@umn.edu)

## **Abstract.**

It has been known for nearly 20 years that the pseudo phase-space density profile of equilibrium simulated dark matter halos,  $\rho(r)/\sigma^3(r)$ , is well described by a power law over 3 decades in radius, even though both the density  $\rho(r)$ , and the velocity dispersion  $\sigma(r)$  deviate significantly from power laws. The origin of this scale-free behavior is not understood. It could be a dynamical attractor that represents an emergent property of self-gravitating collisionless systems, or it could be a mere coincidence. To address the question we work with the second derivative of the Jeans equation, which, under the assumptions of (i) Einasto density profile, (ii) linear velocity anisotropy - density slope relation, and (iii)  $\rho/\sigma^3 \propto r^{-\alpha}$ , can be transformed from a differential equation to a cubic algebraic equation. Relations (i)-(iii) are all observed in numerical simulations, and are well parametrized by a total of 4 or 6 model parameters. We do not consider dynamical evolution of halos; instead, taking advantage of the fact that the algebraic Jeans equation for equilibrium halos puts relations (i)-(iii) on the same footing, we study the (approximate) solutions of this equation in the 4 and 6 dimensional spaces. We argue that the distribution of best solutions in these parameter spaces is inconsistent with  $\rho/\sigma^3 \propto r^{-\alpha}$  being an attractor, and conclude that the scale-free nature of this quantity is likely to be a fluke.

---

## Contents

<b>1</b>	<b>Introduction</b>	<b>1</b>
<b>2</b>	<b>Summary of our analysis methods</b>	<b>2</b>
<b>3</b>	<b>Anisotropic constrained Jeans (ACJ) equation</b>	<b>4</b>
3.1	Second derivative of the ACJ equation	5
3.1.1	Single Einasto algebraic (SEA) equation	5
3.1.2	Triple Einasto algebraic (TEA) equation	6
3.1.3	Figure of merit for evaluating the solutions	6
3.2	Grid-based search for approximate solutions	7
3.2.1	SEA equation	7
3.2.2	TEA equation	10
<b>4</b>	<b>The <math>r</math> dependence of <math>\rho/\sigma^3</math> from the anisotropic unconstrained Jeans equation</b>	<b>12</b>
4.1	Integrating the Jeans equation	12
4.2	Least square fitting of $\rho/\sigma^3$ to a power law	13
<b>5</b>	<b>Conclusions</b>	<b>14</b>
<b>6</b>	<b>Acknowledgement</b>	<b>15</b>
<b>A</b>	<b>Finite difference integration of Jeans Equation</b>	<b>17</b>

---

## 1 Introduction

Dark matter, the dominant mass component of the Universe, is the scaffolding that provides the structure for galaxies and clusters of galaxies. Therefore, understanding the structure of dark matter halos is one of the most important goals of modern cosmology. While the equilibrium structure of stars has been known for about a century, the structure of equilibrium dark matter halos has proven harder to establish. Using the equation of hydrostatic equilibrium and the equation of state for gaseous material allows one to solve for the internal structure of stars. In the case of collisionless dark matter halos, it is not possible to solve the hydrostatic equilibrium equation—also known as the Jeans equation—because the equation of state of dark matter is unknown<sup>1</sup>.

In 2001, an interesting observation was published by [1]. Using N-body simulations, the authors measured mass density,  $\rho(r)$ , and velocity dispersion  $\sigma(r)$ , profiles of equilibrium dark matter halos. The quantity  $\rho/\sigma^3$  turned out to be a power law in radius over about 3 decades, despite the fact that neither density nor the velocity dispersion are power laws, but in fact significantly deviate from a scale-free form. Since then, it has been confirmed by a

---

<sup>1</sup>The equation of state referred to here and other similar contexts in the literature is not the same as the relativistic equation of state,  $w = 0$ , for cold dark matter, used in the cosmological context. Here, the equation of state refers to the relation between mass density  $\rho$ , and dynamically generated "pressure"  $P$  of dark matter, where  $P = \rho\sigma^2$ , and  $\sigma$  is the velocity dispersion.

number of studies that dark matter halos formed in cosmological N-body simulations [2–11], halos computed through an iterative collisionless spherical collapse [12], and even galaxies and clusters formed in the real Universe [13, 14] are well characterized by a power law,

$$\frac{\rho(r)}{\sigma^3(r)} \propto r^{-\alpha}. \quad (1.1)$$

Because this quantity has the dimensions of phase-space density, it has been nicknamed pseudo phase-space density.

Several papers made attempts to shed light on its origin [12, 15–17]. In the meantime, others continued to address the more general question of how to understand the structure of dark matter halos that develops so robustly in simulations [18–22]. [23] proposed a theoretical derivation for the differential energy distribution of self-gravitating relaxed collisionless matter. Based on the principles of statistical mechanics, they proposed the most likely steady-state configuration of these systems. Their result, DARKexp, forms a one shape parameter family, with  $\phi_0$  characterizing the dimensionless depth of the central gravitational potential. DARKexp gives very good fits to the density profiles [4, 24] and, more importantly, to the differential energy distributions of simulated dark matter halos [4, 25]. It also fits well the density profiles of observed equilibrium galaxy clusters [26]. It was shown in [27] that the  $\rho/\sigma^3$  profiles of the DARKexp family are close to, but not exactly power laws for many values of  $\phi_0$ , suggesting that it may not be a universal feature of relaxed systems. Hints of non-universality of this quantity have also been noted in other papers [8, 28, 29].

Recently, [30] challenged the physical origin of the pseudo phase-space density. They consider 1D self-similar fluid collapse, following closely an earlier study by [31]. The authors follow the evolution of gas entropy, whose definition is effectively the same as that of the pseudo phase-space density,  $\rho/\sigma^3$ . Because they are dealing with gas, their treatment cannot incorporate velocity anisotropy, which is measured to be non-zero in numerical dark matter simulations [32–34], as well as some observations of galaxies and galaxy clusters [35–37], and stellar and globular cluster populations in the Milky Way [38].

This paper is a further attempt to understand  $\rho/\sigma^3$ : is there some physical principle behind its power law nature, or is it a mere coincidence. Demonstrating the existence of an underlying physical principle will have important implications for our understanding of self-gravitating collisionless systems. Here, we do not address the possible physical meaning of  $\rho/\sigma^3$ , but instead assume that if one exists, the final equilibrium state of halos will satisfy eq. (1.1).

Our approach differs significantly from that of [30]. While these authors dealt with evolution of isotropic gaseous material, the present work does not consider halo evolution, and instead concentrates on the equilibrium state of halos, where velocity anisotropy plays an important role. Though our methods are very different, our conclusions are essentially the same as theirs: pseudo phase-space density is unlikely to have fundamental physical interpretation, and hence cannot help in the understanding of dark matter halos.

## 2 Summary of our analysis methods

Because we are dealing with equilibrium dark matter halos, the starting point of our analysis is the Jeans equation, a statement of hydrostatic (or, mechanical) equilibrium for collisionless matter. Based on the results of N-body simulations, all the quantities characterizing the spherically averaged equilibrium halos, namely (i) the density profile, (ii) velocity anisotropy

profile, and (iii) pseudo phase-space density profile can be modelled, to a good approximation, as simple analytic relations, with a total of 4 or 6 parameters, depending on how the density profile is represented.

One can make even stronger statements regarding (i) and (iii), going beyond fitting functions to simulations.

The density profiles of relaxed systems are given by a theoretically derived DARKexp, whose radial profile shape is known exactly. For  $\phi_0 \approx 4.5$ , this shape is very closely matched by Einasto profiles, which is why these fit simulated halos very well. In section 3.2.1 we represent density profiles by Einasto profiles, giving us a total of 4 models parameters for (i)-(iii). In section 3.2.2 we assume the density profiles can come from a wider range of DARKexp models, and represent them with 3 Einasto segments, parametrized by 3 parameters, giving us a total of 6 model parameters for (i)-(iii).

If eq. (1.1) stems from some emergent property of collisionless Newtonian gravity, and is a genuine dynamical attractor, then one expects this form to be very closely adhered to by equilibrium dark matter halos. Put differently, it would be pointless to try to explain the radial dependence of  $\rho/\sigma^3$  if it is not a nearly exact power law. In this paper we do not study dynamical evolution of halos, and so do not deal directly with dynamical attractors. We explain the principle behind our analysis later in this section.

The only one of the relations (i)-(iii) that does not have a nearly exact form is the velocity anisotropy profile, (ii). Here we have to rely on simulations. Fortunately, [32] and [33] have shown based on a variety of initial conditions, that equilibrium halos have a tight linear relation between velocity anisotropy  $\beta$ , and the double logarithmic density profile slope,  $\gamma$ . [32] give a range of parameters characterizing that relation, while [33] present a single set of best fitting parameters. We use both of these results in our analysis.

At the end of their dynamical evolution, simulated halos attain a state where all three relations, (i)-(iii), have *nearly* exact parametric forms, represented with 4 or 6 parameters. The values of these parameters have been measured from simulations; let us call them collectively as parameter set (a). In addition to (a), one can define another parameter set, (b), which for the same set of parametric relations, solves the Jeans equation with the smallest residuals.

It is not a foregone conclusion that (a) and (b) are the same set. First, let us consider a situation—possibly hypothetical—where eq. (1.1) is a dynamical attractor. The premise of our analysis is that in this case, the two sets of parameters will be the same, i.e. evolution will find the parameter set for which  $\rho/\sigma^3$  is as close to a power law as it can be. On the other hand, if  $\rho/\sigma^3$  being an approximate power law in simulated halos is a coincidence, there is no reason why dynamical evolution would drive halos towards a state where eq. (1.1) is satisfied as best as possible. If eq. (1.1) is not a dynamical attractor, parameters sets (a) and (b) need not be the same.

To assess the similarity of the two parameter sets (a) and (b) we evaluate the quality of solutions from a wide and finely sampled region of the model parameter space. Since all 3 relations, (i)-(iii), are of equal importance, one should treat them equally. This is not possible if one assumes exact forms for (i) and (ii), and then integrates the Jeans equation to get (iii). Fortunately, there is a way to place (i)-(iii), and their associated 4 or 6 model parameters, on the same footing. In section 3.1 we show that the second derivative of the Jeans equation, combined with an Einasto profile, can be converted to a cubic algebraic equation. We then calculate how well each set of parameters satisfies this algebraic equation. In contrast to the integration of the Jeans equation, the algebraic equation does not single out  $\rho/\sigma^3$ .

We call the parameter set, (b), that satisfies this equation as best as possible, the ‘kinematic attractor’. (We quantify how we find best solutions in section 3.1.3.) It is distinct from the concept of dynamical attractor because our kinematic attractor is not obtained as the end result of dynamical evolution. To find a dynamical attractor one would need to follow halos’ evolution in a large parameter space capable of describing all the possible functional forms of density, velocity anisotropy, and  $\rho/\sigma^3$  that arise during evolution. Instead, we work in 4 or 6 parameter space, just sufficient to characterize the equilibrium end point of evolution. A further distinction is that, as defined in this paper, the dynamical attractor consists of eq. (1.1) only, while our kinematic attractor consists of a combination of all three parametric properties, (i)-(iii), of equilibrium halos.

Since (i)-(iii) have been observed in simulations, we know that a rough agreement between sets (a) and (b) is guaranteed. Therefore, in order to provide support for eq. (1.1) having a physical meaning, we are looking for a better than a rough agreement. In that case, we also expect the kinematic attractor, set (b), to form a well defined and isolated trough in the parameter space, and be stable against small changes in parametrization, like changing from 4 to 6 parameters.

The analysis just described is carried out in section 3. For completeness, in section 4 we return to the more traditional method of solving the Jeans equation, i.e., we integrate it directly, without assuming that  $\rho/\sigma^3$  is a power law, and compare the resulting  $\rho/\sigma^3$  to a power law. We do this only for a limited set of best solutions found in section 3.

### 3 Anisotropic constrained Jeans (ACJ) equation

In this section we will work with the second derivative of the Jeans equation, and parametrized forms of the density profile, velocity anisotropy profile, and power law profile of pseudo phase-space density.

We start with the anisotropic Jean’s equation,

$$\frac{d}{dr} \left\{ \frac{\rho(r)\sigma^2(r)}{3-2\beta(r)} \right\} + \frac{2\beta(r)}{3-2\beta(r)} \frac{\rho(r)\sigma^2(r)}{r} = -G\rho(r) \frac{M(r)}{r^2} \quad (3.1)$$

where  $M(r)$  is the mass enclosed within radius  $r$ ,  $\rho$  is the density at that radius,  $\sigma$  is the total velocity dispersion<sup>2</sup>, and  $\beta$  is the anisotropy, defined using the tangential,  $\sigma_t^2 = \frac{1}{2}(\sigma_\phi^2 + \sigma_\theta^2)$ , and radial velocity dispersions of a dark matter halo:  $\beta(r) \equiv 1 - \frac{\sigma_t^2}{\sigma_r^2}$ . We define dimensionless variables  $x \equiv r/r_0$  and  $y \equiv \rho/\rho_0$ , and reduce the number of functions in eq. (3.1) by invoking the power law nature of the pseudo phase-space density profile,  $\rho/\sigma^3 = (\rho_0/\sigma_0^3)(r/r_0)^{-\alpha}$ :

$$\frac{-x^2}{y} \left\{ \frac{d}{dr} \left[ \frac{y^{5/3}x^{2\alpha/3}}{3-2\beta(r)} \right] + \frac{2\beta(x)}{3-2\beta(x)} y^{\frac{5}{3}} x^{\frac{2\alpha}{3}-1} \right\} = BM(x) \quad (3.2)$$

where  $B = G/r_0 v_o^2$ . Using the assumption of eq. (1.1) leads to Jeans equation constrained. From now on, ACJ refers to anisotropic constrained Jeans equation.

---

<sup>2</sup>While some authors use just the radial velocity dispersion in eq. (1.1), we use the total dispersion,  $\sigma^2 = \sigma_r^2 + \sigma_\phi^2 + \sigma_\theta^2$ .

### 3.1 Second derivative of the ACJ equation

We differentiate eq. (3.2) with respect  $x$ , as was done in [1], then following [39] and [40], we differentiate it again with respect to  $x$ , arriving at

$$\begin{aligned}
(2\alpha + \gamma - 6) & \left[ \frac{2}{3}(\alpha - \gamma) + 1 \right] (2\alpha - 5\gamma) \\
& = 15\gamma'' + 3\gamma'(8\alpha - 5\gamma + 4\beta + 12\beta\theta b_1 - 5) \\
& \quad - 3\theta[b_1(4\alpha^2 + \gamma^2 - 8\alpha\gamma + 8\alpha + 7\gamma - 15)] \\
& \quad - 3\theta^2[6b_1b_2(\alpha - \gamma + 1)] \\
& \quad - 3\theta^3[b_3(54\beta + 144\beta^2 + 24\beta^3)] \\
& \quad - 3\theta'[6b_1(\alpha - \gamma + 1) + 9b_1b_2\delta] - 3\theta''(3b_1)
\end{aligned} \tag{3.3}$$

where  $\gamma = -d \ln y / d \ln x$  is the double logarithmic density slope,  $\theta = d \ln \beta / d \ln x$ ,  $b_1 = 2\beta/(3 - 2\beta)$ ,  $b_2 = (3 + 2\beta)/(3 - 2\beta)$ ,  $b_3 = (3 - 2\beta)^{-3}$ , and the primes indicate logarithmic derivatives. Using a range of initial conditions for collisionless N-body simulations, [32, 33] find that after equilibrium is achieved, all the halos end up having very similar shapes of the velocity anisotropy. All are well described by a linear relation<sup>3</sup> between  $\beta$  and  $\gamma$ :

$$\beta(r) = \eta_1 + \eta_2\gamma(r). \tag{3.4}$$

This allows us to compute the logarithmic derivatives of  $\theta$ :

$$\theta = -\frac{\eta_2}{\beta}\gamma' \tag{3.5a}$$

$$\theta' = -\frac{\eta_2}{\beta} \left\{ \frac{\eta_2}{\beta}(\gamma')^2 + \gamma'' \right\} \tag{3.5b}$$

$$\theta'' = -\frac{\eta_2}{\beta} \left\{ \frac{2(\gamma')^2\eta_2^2\gamma}{\beta^3} + 2\gamma'\gamma'' + \frac{\gamma''}{\beta^2}\eta_2\gamma + \frac{\gamma'''}{\beta} \right\} \tag{3.5c}$$

Eq. (3.3) is a second order differential equation in  $\gamma$  and  $\theta$ . It can be further expanded by using logarithmic derivatives in eq. (3.5), thereby converting the eq. (3.3) into a third order differential equation in one variable only,  $\gamma$ . Due to the complexity of eq. (3.3) and (3.5), we are not showing the combined expression obtained after assembling all the parts together.

#### 3.1.1 Single Einasto algebraic (SEA) equation

The logarithmic density  $\gamma$  can take many forms; a simple analytical expression that fits N-body density profiles well and is commonly used in the literature is the Einasto profile [41, 42]:

$$\gamma = Ax^p, \tag{3.6}$$

where  $A$  is a normalization constant. It has an interesting, and useful property that all its logarithmic derivatives have a linear dependence on  $\gamma$ :

$$\gamma' = Ap x^p = p\gamma \tag{3.7a}$$

$$\gamma'' = Ap^2 x^p = p^2\gamma \tag{3.7b}$$

$$\gamma''' = Ap^3 x^p = p^3\gamma. \tag{3.7c}$$

---

<sup>3</sup>Note that the sign in front of  $\eta_2$  is different from that in [32] and [33] because our definition of  $\gamma$  has a minus sign, while theirs does not.

We take advantage of this property of the Einasto profile. In eq. (3.3) and (3.5) we eliminate all derivatives of  $\gamma$  by replacing them with their counterparts in eq. (3.7). This converts differential eq. (3.3) into an algebraic equation of cubic order. From now on, we will refer to it as the single Einasto algebraic (SEA) equation that consists of a collection of eq. (3.3) - (3.7). It depends on 4 parameters: the power law slope of the pseudo phase-space density  $\alpha$ , the two velocity anisotropy parameters,  $\eta_1$ ,  $\eta_2$  and the Einasto parameter  $p$ .

### 3.1.2 Triple Einasto algebraic (TEA) equation

Though Einasto profiles fit N-body dark matter halo density profiles quite well, they are still only fitting functions. DARKexp models have the advantage of being theoretically derived from fundamental statistical mechanical principles. They also fit the density profiles, and the energy distributions of N-body halos very well. It is not surprising that they resemble Einasto profiles for a certain range of DARKexp shape parameter  $\phi_0$ . DARKexp density profiles do not have an analytic expression, but since for the relevant range of  $\phi_0$  they are not too different from the Einasto shape, DARKexp can be approximated by three Einasto segments, with three different slopes  $p_1$ ,  $p_2$  and  $p_3$ , respectively. The profiles we use cover 3 decades in radius, from  $x = 10^{-2}$  to  $x = 10^1$ , and  $x = 1$  corresponds to the radius where  $\gamma = 2$ , i.e. has the isothermal slope.

$$\gamma(x) = \begin{cases} 2 \times 10^{1.3(p_1-p_2)} x^{p_1}, & \log x \leq -1.3 \\ 2 x^{p_2}, & -1.3 \leq \log x \leq 0 \\ 2 x^{p_3}, & 0 \leq \log x. \end{cases} \quad (3.8)$$

The continuity conditions are derived at  $\log x = -1.3$  and  $\log x = 0$  by forcing the density slopes  $\gamma$  to be equal at these two points, with the help of a constant multiplier in the logarithmic units. We also require that  $p_2 \leq p_1$ , in accordance with the shape of DARKexp density profiles [25].

When eq. (3.8) is substituted in to the eq. (3.3), the final equation becomes a function of 6 model parameters: the power law slope of the pseudo phase-space density  $\alpha$ , the two velocity anisotropy parameters,  $\eta_1$ ,  $\eta_2$ , and three Einasto parameters  $p_1$ ,  $p_2$  and  $p_3$ , which collectively approximate DARKexp. We call it the triple Einasto algebraic (TEA) equation, which consists of eq. (3.3) - (3.8).

### 3.1.3 Figure of merit for evaluating the solutions

If the simple analytical assumptions—eq. (1.1), (3.4), and eq. (3.6) or eq. (3.8)—are exactly correct, then the SEA and TEA equations will be exactly true at all radii,  $x$ . However, this is not the case for any set of 4 or 6 parameters. To estimate how well any given set of parameters solves the two equations over the 3 decades in radius, we calculated the normalized absolute difference between the left hand side (LHS) and the right hand side (RHS) of the equations and averaged these values over the 3 decade range of radii. The resulting value, which we call  $\delta$ , is defined as,

$$\delta = \left\langle \frac{|LHS - RHS|}{\sqrt{(LHS^2 + RHS^2)/2}} \right\rangle_x \quad (3.9)$$

After scanning a large portion of the parameter space, we will identify regions that represent best solutions of the two equations, and compare the corresponding parameter values to those found in computer simulations. These best solutions, i.e., the global minima

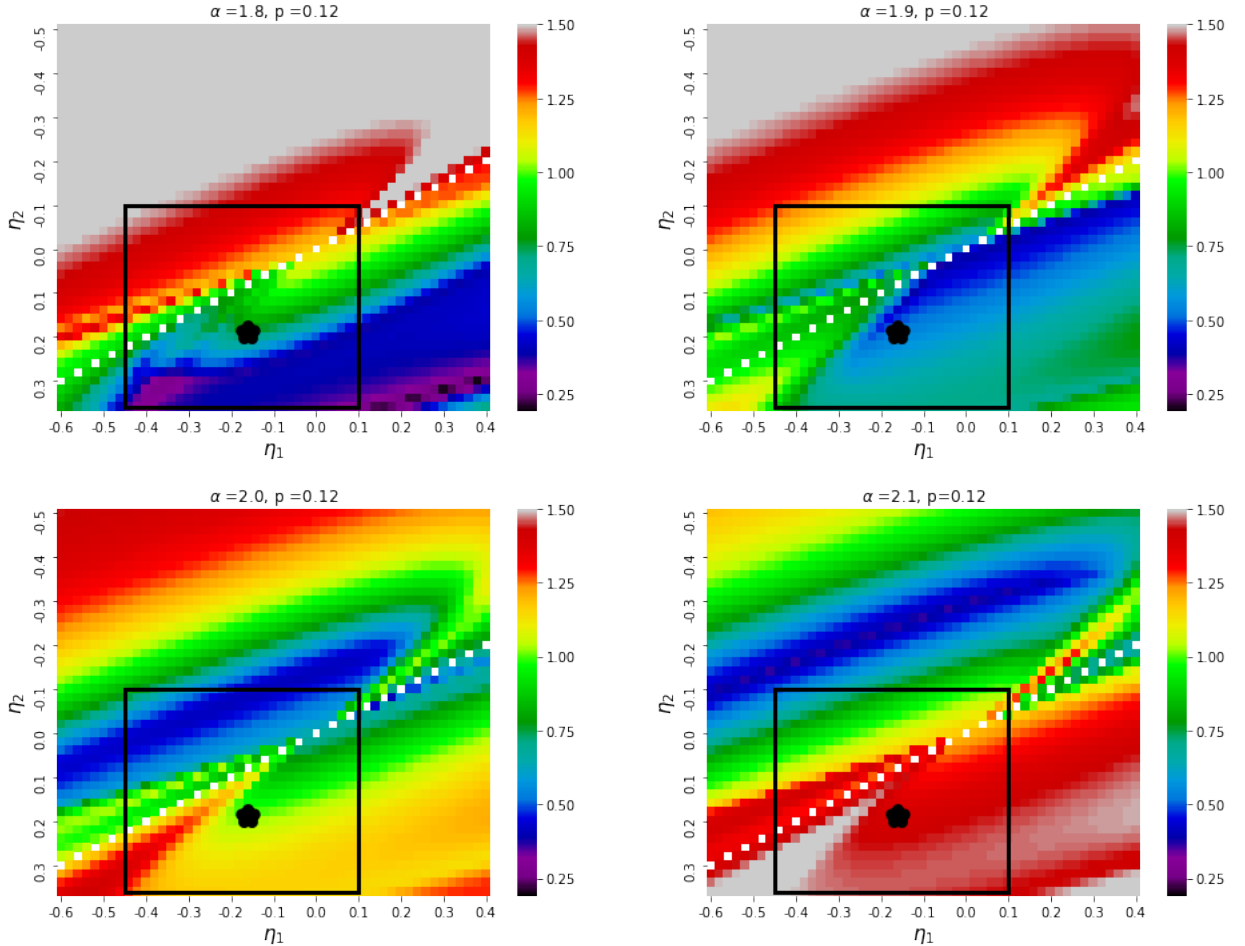


**Figure 1.** Heat maps of  $\delta$  values as a function of velocity anisotropy parameters,  $\eta_1$  and  $\eta_2$ , for a single Einasto density profile, eq. (3.6), with the density slope value,  $p = 0.12$ , corresponding to the lowest  $\delta$ . The four panels show four values of  $\alpha$  values, 1.8, 1.9, 2.0 and 2.1. The black rectangular regions outline  $\eta_1$  and  $\eta_2$  values obtained in [32], and are the limits of regions plotted in figure 3. The black dot marks the parameters presented in [33].

of  $\delta$  found for the two equations are the kinematic attractors. For the TEA equation, we will then integrate the anisotropic unconstrained Jeans equation, eq. (3.1), in section 4.

### 3.2 Grid-based search for approximate solutions

#### 3.2.1 SEA equation

Here, we consider the single Einasto profile of eq. (3.6), resulting in a four dimensional parameter space. The parameter ranges covered are:  $1.8 \leq \alpha \leq 2.2$ ,  $-0.60 \leq \eta_1 \leq 0.40$ ,  $-0.5 \leq \eta_2 \leq 0.36$ ,  $0.02 \leq p \leq 0.3$ , with step size of 0.02 for all parameters. Our parameter range for  $\alpha$  values is wider than what is found in the literature, which generally span  $\sim 1.85 - 1.96$ . The range of density profile slopes is also somewhat wider. The velocity anisotropy parameter ranges encompass those found in N-body simulations, as analyzed in [32].

We start by calculating the figure of merit,  $\delta$ , eq. (3.9), at every location in the four dimensional parameter space. Given our step size and parameter limits, we consider a total

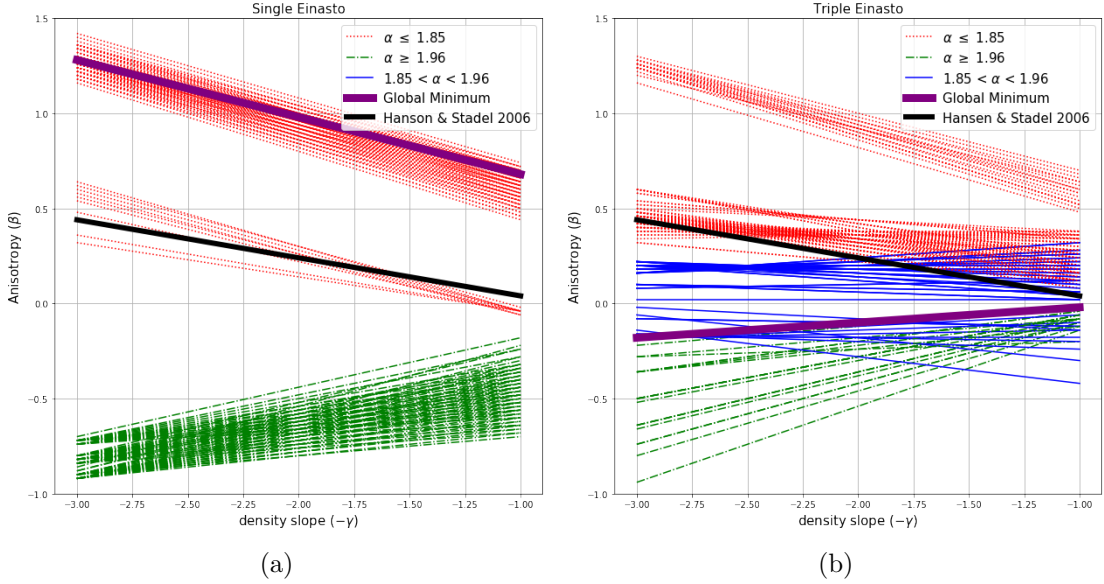


**Figure 2.** The anisotropy-density relation  $\beta$  for the lowest 150  $\delta$  values found in the (a) 4 dimensional parameter space of the single Einasto profile, and (b) hexa-dimensional space of the triple Einasto profile. The black line in both panels assumes the anisotropy parameters from [33], of simulated dark matter halos. The thick purple lines are the global minima of our two searches. The profiles are colored by their value of  $\alpha$ , as indicated in the legend.

of around  $5 \times 10^5$  parameter sets. The parameter sets with the lowest  $\delta$  values correspond to the best solutions to the SEA equation. Figure of merit  $\delta$  is always greater than zero, meaning that no solution is exact. As was pointed out in section 2, the advantage of using the second derivative of the Jeans equation is that, by design, it contains no information about which one of the three analytic assumptions—density, anisotropy, or  $\rho/\sigma^3$  profile, or what combination of the three—is the reason for  $\delta$  being non-zero. In the rest of this subsection we study the interdependence of these parameters, examine the properties of the best solutions, and compare them to those of dark matter halos found in simulations.

To display the solution space, we chose the density profile slope  $p$  corresponding to the lowest global  $\delta$  value ( $p = 0.12$ ), and plot 4 cuts through the remaining 3D parameter space, corresponding to 4 values of  $\alpha$ : 1.8, 1.9, 2.0 and 2.1; see figure 1. The color scale in these heat maps is the same for all 4 panels. The gray color indicates values of  $\delta$  outside our range. The black box outlines the anisotropy parameters given in [32], while the black dot marks the single set presented in [33]; both are based on simulated halos.

The pattern revealed in these approximate solutions is complicated. There is a symmetry axis outlined by white pixels, where the denominator of  $\delta$  is zero for some values of  $x$ . It goes roughly diagonally through all 4 panels, and the color pattern is inverted across the axis. The trough of minima is to the right of this axis for  $\alpha = 1.8 - 1.9$ , and shifts to the left for large values of  $\alpha$ .

The diagonally stretched pattern of  $\delta$  values seen in these panels state that if  $\eta_1$  is increased by a small amount, and  $\eta_2$  is simultaneously decreased, or vice versa, the  $\delta$  value of the new  $\beta - \gamma$  relation will stay approximately the same. Segments of such modified linear  $\beta - \gamma$  relations can be stitched together to make a new, somewhat non-linear relation, which will also have similar  $\delta$ . This means that our analysis indirectly includes curved  $\beta - \gamma$

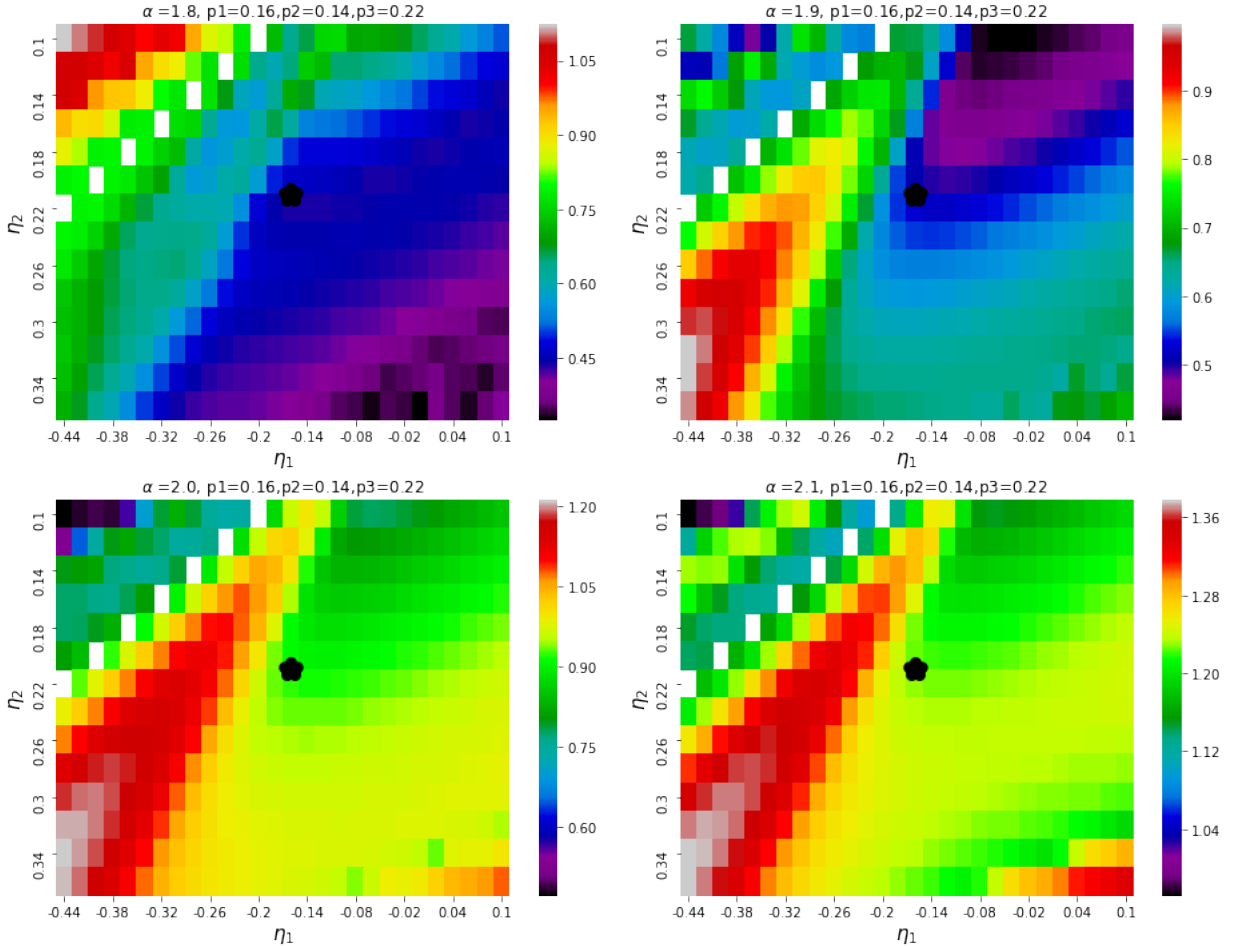


**Figure 3.** Similar to figure 1. Heat maps of  $\delta$  values as a function of velocity anisotropy parameters,  $\eta_1$  and  $\eta_2$ , for a triple Einasto density profile, eq. (3.8), with the density slopes,  $p_1 = 0.16$ ,  $p_2 = 0.14$  and  $p_3 = 0.22$ , corresponding to the lowest  $\delta$ . The density profiles are shown in figure 4b. Note that the color ranges are different in the four panels.

relations, as long as they stay within confines of the parameters defined by [32].

The global  $\delta$  minimum is at  $(\alpha, p, \eta_1, \eta_2) = (1.80, 0.12, 0.38, 0.30)$  in table 1, and does not correspond closely to the parameters of the simulated halos. Specifically, the anisotropies are too large, even exceeding  $\beta = 1$  (which is not allowed because of the definition of  $\beta$ ), the Einasto density profile slope,  $p$ , is too small, and the slope of the pseudo phase-space density profile,  $\alpha$  is a little shallower than the range seen in simulations. The fact that the parameter set of the kinematic attractor does not coincide well with the one observed in simulations is an indication that  $\rho/\sigma^3$  is not as close to a power law as it could have been, and hence does not have a physical significance.

Because the analytical forms we assume for the density and velocity anisotropy profiles are approximations only, to get a better sense of how well SEA equation is satisfied, we consider a wider range of solutions, instead of just the global minimum. To that end, we select 150 parameter sets with the lowest values of  $\delta$ , and study their properties. This is a tiny fraction of the total number of parameter sets we computed  $\delta$  for, and so all of these

can still be considered as very good solutions. While 150 is an arbitrary number, using a different small fraction of the total would not change our conclusions.

The best 150 solutions in the space of anisotropy-density relation are displayed in figure 2a. The global minimum is the thick purple line, and is very different from the anisotropy-density relation found in simulations. The thin lines (150 solutions) are color coded by their  $\alpha$  value. The range found in simulations,  $1.85 \leq \alpha \leq 1.96$  (blue) does not occur in this set.

As we argued in section 2, if  $\rho/\sigma^3$  being a power law had a physical origin, the lowest  $\delta$  solution, the kinematic attractor, would coincide closely with the parameter set found in simulations, and there would have been a trough of low  $\delta$  values around the latter parameter set, as one would expect for any well defined minimum in a parameter space.

### 3.2.2 TEA equation

In this section we extend the range of density profiles we consider, by including profiles that resemble DARKexp, which can be approximated by three joined Einasto-like segments, eq. (3.8).

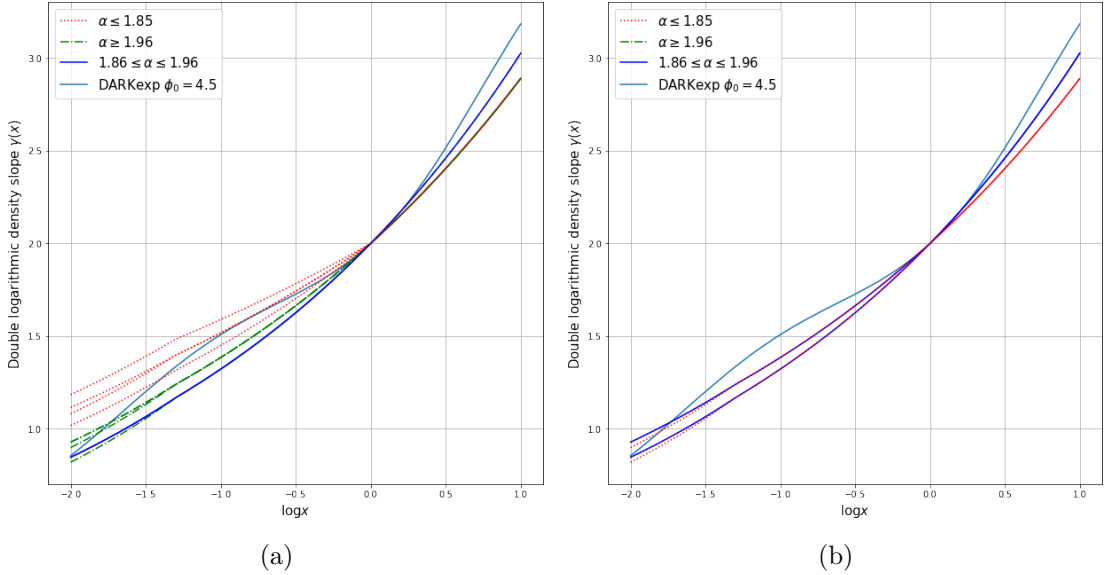
The corresponding hexa-dimensional parameter space we search spans the same range for  $\alpha$ ,  $\eta_1$  and  $\eta_2$  as in section 3.2.1. The values of the slope of the two Einasto segments of the density profile at smaller radii,  $p_1$  and  $p_2$ , cover the same range as  $p$ , but the segment that applies to larger radii spans  $0.16 \leq p_3 \leq 0.24$ , because the density profile is expected to be steeper there. We impose an additional constraint that  $p_2 \leq p_1$ , as indicated by the shape of DARKexp density profiles. The step size in each of the 6 dimensions is 0.02, so the total number of parameter sets we consider is nearly  $2.5 \times 10^7$ .

Figure 3 is similar to figure 1, but only shows  $\eta_1$  and  $\eta_2$  ranges that are indicated by black rectangles in the latter figure. This is the velocity anisotropy range found in simulations [32]. The 4 panels correspond to the same four  $\alpha$  values as in that figure, while the 3 values of the density profile slopes of triple Einasto are those that correspond to the lowest  $\delta$  value.

Just like the  $\delta$  maps in figure 1, the ones in figure 3 also show complicated patterns. (Note that the color scale is different in the four panels.) The global  $\delta$  minimum, i.e., the kinematic attractor in this case is at  $(\alpha, p_1, p_2, p_3, \eta_1, \eta_2) = (1.94, 0.2, 0.18, 0.16, 0.06, -0.08)$ , in table 1. Its parameter values are roughly consistent with, but are not the same as those found in simulations. The  $\alpha$  value is a little too large, the density profile is only marginally well approximated by either Einasto or DARKexp, and the anisotropy  $\beta$  is mildly tangentially anisotropic at large radii in contrast to the radially anisotropic velocity profiles of simulated halos.

Figure 2b shows the anisotropy-density relation for the 150 best solutions. The global minimum is shown as a thick purple line. The average  $\beta - \gamma$  relation from simulations [33] is plotted for reference as the thick black line. Most, if not all of the best 150 solutions have properties different from those of simulated equilibrium halos. All green lines, and the thick purple line have the anisotropy-density slope opposite to that seen in simulations, and  $\alpha$  values that are larger than those seen in simulations,  $\alpha \geq 1.96$ . The solutions represented by red lines have  $\alpha$  values that are too small,  $\alpha \leq 1.85$ . Furthermore, many of these have  $\beta > 1$  in the relevant range of density slopes. The solutions that have  $\alpha$  in the observed range,  $1.85 \leq \alpha \leq 1.96$  (blue lines) have approximately isotropic velocity distributions at all radii, and are thus only marginally consistent with simulations.

Figure 4a shows the density profile slopes vs. log radius, for the 150 best solutions, color coded by  $\alpha$  as in figure 2b, and figure 4b plots the subset of these 150 solutions that are within [32] anisotropy range. Though we allowed a rather broad range of slopes for  $p_1$ ,  $p_2$  and  $p_3$ ,



**Figure 4.** Double logarithmic density slope  $\gamma$  as a function of logarithmic scaled radius,  $\log(x)$ . In both panels, the thin lines are the 150 best solutions from section 3.2.2, color coded by  $\alpha$ . DARKexp  $\phi_0 = 4.5$  density profile is plotted as light blue. (a) Solutions, regardless of anisotropy parameters; (b) Solutions with anisotropy parameters in the [32] range. There is considerable overlap of the curves, so in all cases a single profile actually represents many profiles.

the best solutions are all clustered around a narrow range of values, resulting in considerable overlap of profiles in the figure. These values are such that  $p_1 \approx p_2 \approx 0.16 - 0.18$ , and  $p_3 \approx 0.18 - 0.20$ . In other words, even though the density profile had the option of deviating from an Einasto form, the best solutions still have  $p_1 \approx p_2 \approx p_3$ . The closest DARKexp has  $\phi_0 = 4.5$ , and is represented as a light blue line. So the density profiles corresponding to best solutions are similar to, but not the same as those found in N-body simulations.

To sum up, the parameter set found in simulations is (A) close to, but (B) not very close to the best solution to the anisotropic constrained Jeans equation. This is clear from the cross-sections of the full parameter space presented in figure 3, as well as the closer examination of a small subset of 150 best solution, in figures 2b, 4a. Statement (A) is a posteriori conclusion, which was already shown to be the case by [1]. Statement (B) suggests that the approximate power law nature of  $\rho/\sigma^3$  found in simulations is a coincidence.

A further conclusion drawn from these results argues against eq. (1.1) being a dynamical attractor. If it were one, we would expect the parameters of the kinematic attractors using single Einasto (section 3.2.1) and triple Einasto (section 3.2.2) to be similar (see the first two rows in table 1). This is not the case. While the density profiles in both cases are both Einasto-like (for the triple Einasto  $p_1 \approx p_2 \approx p_3$ ), the slopes are different, and the power law exponents  $\alpha$ , and the velocity anisotropies are very different. Thus, a relatively small change in the parametrization of the problem significantly changes the parameters of the global minimum. Thus the kinematic attractor is unstable, implying that eq. (1.1) is unlikely to be a dynamical attractor.

## 4 The $r$ dependence of $\rho/\sigma^3$ from the anisotropic unconstrained Jeans equation

In section 3 we assumed the power law nature of the phase-space density profile, eq. (1.1) and looked for approximate solutions of the Jeans equation, where any of the 3 radial profiles—density, velocity anisotropy, and  $\rho/\sigma^3$ —could deviate from their simple forms. However, the nature of that analysis did not allow us to examine the magnitude and radial dependence of these deviations.

In this section, rather than assuming eq. (1.1), we compute the radial dependence of  $\rho/\sigma^3$  by solving the unconstrained anisotropic Jeans equation, eq. (3.1), for  $\sigma(r)$ . The density and anisotropy radial profiles have the same forms as before. We then fit the computed  $\rho/\sigma^3$  with a power law of the form  $x^{\alpha_{LSQ}}$  over 3 decades in radius, and compare  $\alpha_{LSQ}$  to the power law parameter  $\alpha$  from section 3.2.2. This is done to demonstrate explicitly how well the parameter sets of best solutions to TEA equation found in section 3.2.2 follow eq. (1.1), under the constraint (not imposed in section 3) that the density and velocity anisotropy follow the exact parametric relations. It should be noted that this analysis was not repeated for SEA equation because the best  $\alpha$  and  $p$  ranges found in section 3.2.1 did not agree with the values in the literature.

### 4.1 Integrating the Jeans equation

The unconstrained Jeans equation, eq. (3.1), depends on  $\beta(\gamma)$ ,  $\rho(r)$  and  $\sigma(r)$ . We use the parameter sets  $(p_1, p_2, p_3, \eta_1, \eta_2)$  obtained in section 3.2.2 to numerically integrate eq. (3.1). Since we are now dealing with the density profile itself, instead of its double logarithmic slope,  $\gamma$ , we need to convert eq. (3.8) to  $\rho(x)$ , i.e., impose continuity conditions at  $\log(x) = -1.3$  and  $\log(x) = 0$ . The density profile  $\rho(x)$  becomes:

$$\rho(x) = \begin{cases} \exp\left(\frac{-2x^{p_1}}{p_1} 10^{1.3(p_1-p_2)}\right), & \log x \leq -1.3, \\ c_1 \exp\left(\frac{-2x^{p_2}}{p_2}\right), & -1.3 \leq \log x \leq 0, \\ c_2 \exp\left(\frac{-2x^{p_3}}{p_3}\right), & \log x \geq 0, \end{cases} \quad (4.1)$$

where constants  $c_1$  and  $c_2$  are given by  $c_1 = \exp(10^{-1.3p_2}[1/p_2 - 1/p_1])$ , and  $c_2 = c_1 \exp(2[1/p_3 - 1/p_2])$ . Figure 5a shows the input density profile (orange curve) obtained for the parameters of the global minimum of section 3.2.2. The density is very smooth, and does not show the discontinuities in our definition of  $\rho$ .

We are now able to solve eq. (3.1) using eq. (4.1) and anisotropy  $\beta(\gamma)$ , following the steps in Appendix A. We impose the boundary condition that  $\sigma = 0$  for large values of  $x$ , and find  $\sigma(r)$ . Figure 5a shows the velocity dispersion profile (blue curve) for parameters of the global minimum obtained in section 3.2.2.

Figure 5b displays the resulting  $\rho/\sigma^3$  (orange curve), together with the  $\rho/\sigma^3$  assumed in section 3.2.2 (green dot-dash line) for the same parameter set. (Vertical normalization is arbitrary, since it was not needed at all when working with the second derivative of the ACJ equation.) The difference between the orange curve and the green dot-dash line shows explicitly by how much the simple assumptions for density, anisotropy and  $\rho/\sigma^3$  profiles fall short of solving the TEA equation. In this case, the difference is not very large.

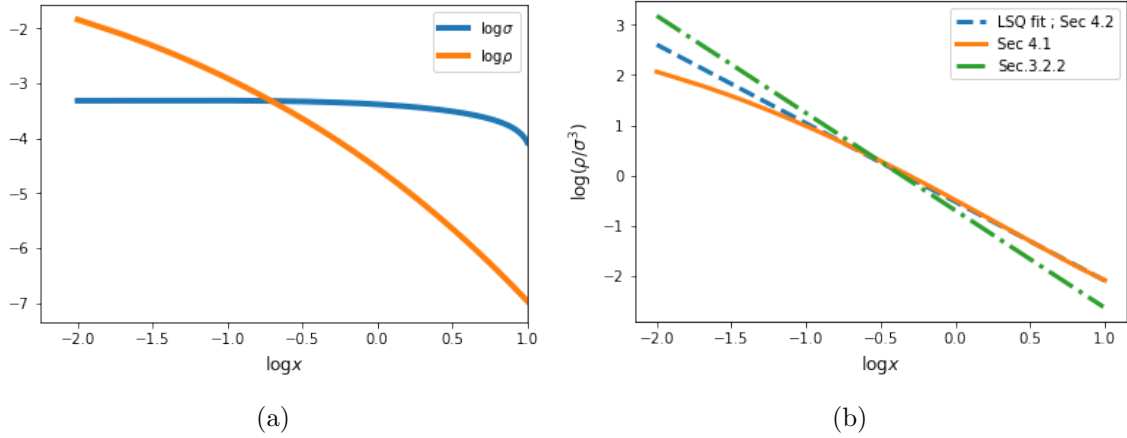


**Figure 5.** (a) Density profile  $\rho(x)$  (orange), eq. (4.1), and velocity dispersion profile  $\sigma(x)$  (blue) for the best solution in section 3.2.2. The vertical normalization is not important and was adjusted to fit both profiles on the same scale. (b) Phase-space density profile, obtained by integrating the unconstrained Jeans equation, for the same system as in left panel (orange), and the line of best fit (blue dashed)  $\alpha_{LSQ} = 1.56$ . The green dot-dash line corresponds to the same system, but obtained using TEA equation in section 3.2.2.

#### 4.2 Least square fitting of $\rho/\sigma^3$ to a power law

To extend this analysis to the 150 best solutions of section 3.2.2, we need to concisely summarize the discrepancy between the power law  $\rho/\sigma^3$  assumed in that section and the non-power law radial profile of  $\rho/\sigma^3$  found in section 4.1. To that end, we fit the latter with a power law, using least squares fitting, and call the resulting slope  $\alpha_{LSQ}$ .

The power law fitted to the orange curve in figure 5b, which was calculated in section 4.1, is shown as the blue dashed line; its  $\alpha_{LSQ} = 1.56$ , the corresponding  $\alpha = 1.94$ .

Next we calculate  $\alpha_{LSQ}$  for the 150 parameter sets with the lowest  $\delta$  values. The difference,  $\alpha - \alpha_{LSQ}$ , provides the natural way to quantify the discrepancy. Figure 6a plots the  $\alpha - \alpha_{LSQ}$ , versus  $\delta$  obtained in section 3.2.2. The green circles and red crosses represent solutions that have anisotropy parameters in the [32] range, and outside of that range, respectively. Only a small fraction of the 150 solutions are consistent with the results of [32] (green points). All but one of these have  $\alpha - \alpha_{LSQ} \sim 1$ , indicating a significant deviation from a good solution. The best solution is the green dot in the lower right corner of the panel with corresponding parameters in table 1. (Note that this is not the same best solution as the lowest value  $\delta$  solution of section 3.2.2.) Its anisotropy parameters ( $\eta_1 = -0.42$  and  $\eta_2 = 0.12$ ) are barely within the range of simulated halos [32], but the corresponding anisotropy profile is tangentially anisotropic in the whole 3 decade radial range.

To show the actual values of the slope of  $\rho/\sigma^3$ , figure 6b plots  $\alpha_{LSQ}$  versus  $\alpha$ , and the light blue line shows the one-to-one correspondence. In all cases the fitted power laws have shallower slopes than slopes obtained in section 3.2.2. As we already mentioned in the previous paragraph, this best solution is inconsistent with the results of N-body simulations.

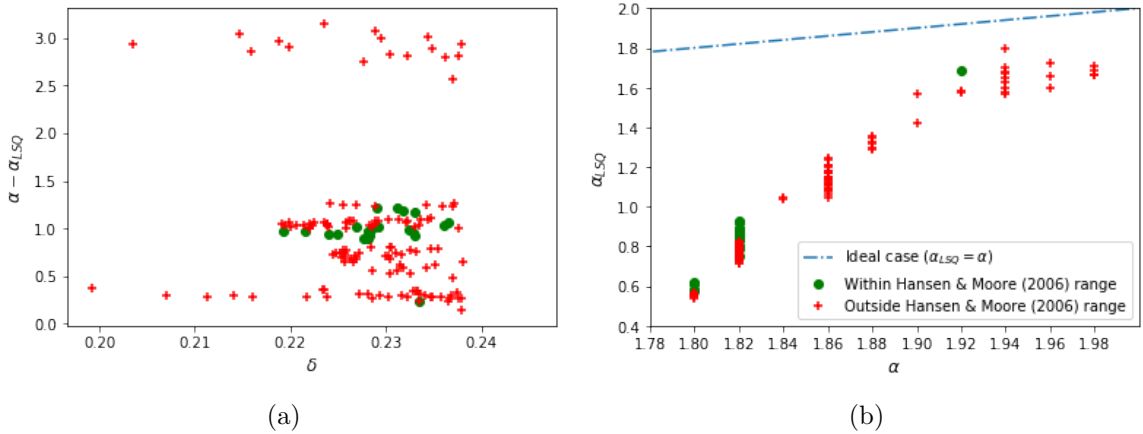


**Figure 6.** The best 150 solutions from section 3.2.2. (a) The difference between  $\rho/\sigma^3$  power law exponents,  $\alpha - \alpha_{LSQ}$  as a function of  $\delta$ , obtained in section 3.2.2. The green circles and red crosses represent solutions with anisotropy parameter values inside and outside, respectively, of the range described in [32]. (b)  $\alpha_{LSQ}$  as a function of  $\alpha$  for the same set solutions, except those with  $\alpha_{LSQ} < 0$ . The dot-dash line represents  $\alpha = \alpha_{LSQ}$ ; (none of the solutions are on that line.)

**Table 1.** Parameter sets of best solutions from sections 3.2.1, 3.2.2 and 4.2

Solution	$\alpha$	$p$	$p_1$	$p_2$	$p_3$	$\eta_1$	$\eta_2$	$\delta$
Global Min (SEA equation)	1.8	0.12	—	—	—	0.38	0.30	0.201
Global Min (TEA equation)	1.94	—	0.2	0.18	0.16	0.06	-0.08	0.199
Best Solution (Section 4.2)	1.92	—	0.2	0.18	0.16	-0.42	0.12	0.233

## 5 Conclusions

It has been known for almost 20 years that the pseudo phase-space density profiles of equilibrium dark matter halos are well approximated by a power law in over  $\sim 3$  decades radius. The main goal of this paper is to determine whether this scale-free behavior could have a physical origin, or is simply a curious coincidence. While we do not address the possible physical meaning of  $\rho/\sigma^3$  being a power law, we assume that if one exists, equilibrium halos will obey the eq. (1.1) relation.

We do not analyze dynamical evolution of halos, and instead work with the final equilibrium halos. We use the Jeans equation of hydrostatic equilibrium, and the two simple parametric relations that describe the radial behavior of the density and velocity anisotropy profiles. Our first analysis assumes these forms, as well as  $\rho/\sigma^3 \propto r^{-\alpha}$ , which are parametrized by a total of 4 or 6 model parameters, depending on whether density profiles are described by a single or triple Einasto profiles. We then search the parameter space, over a sufficiently wide and finely sampled range, for the best solution to the Jeans equation. We call it the kinematic attractor, to distinguish it from the more commonly used concept of dynamical attractor. (Since the equation is overconstrained, only approximate solutions are possible.) Because all three relations are seen in simulations, we already know that parameters describing N-body halos will correspond to reasonably good solutions of the Jeans equation. However, if  $\rho/\sigma^3 \propto r^{-\alpha}$  has a physical origin, we expect N-body halos to correspond to the

best solutions, and expect these to form a well defined, isolated, and stable global minimum trough.

What we actually find is quite different. While the global best solution and the N-body halo parameters are reasonably close to each other, the structure of the solution space is complicated, with no indication of an isolated trough. Furthermore, we find that if the parametrization of the density profile is changed somewhat, from a single to triple Einasto, the parameters of the best solution, and especially those of velocity anisotropy change significantly (table 1), indicating that the global minimum in the solution space is not stable.

Because the parameters describing the density, velocity dispersion and  $\rho/\sigma^3$  radial profiles observed in simulations are not the ones that would result in the  $\rho/\sigma^3$  being closest to a power law, we conclude that the approximate power law nature of the pseudo phase-space density seen in N-body simulations and semi-analytical collapses does not have a physically meaningful origin, and so does not shed light on the effective equation of state of self-gravitating dark matter halos.

Finally, we note that the second derivative of the Jeans equation, first introduced by [12, 39], can have other useful applications, beyond the purpose of this paper. Defining  $f = \text{LHS} - \text{RHS}$ , where the left and right hand sides refer to the Jeans equation itself, one can Taylor expand around any radius  $x_0$ ,

$$f(x) = f(x_0) + (x - x_0) \frac{\partial f}{\partial x} \Big|_{x_0} + \frac{1}{2}(x - x_0)^2 \frac{\partial^2 f}{\partial x^2} \Big|_{x_0} + \dots \quad (5.1)$$

In equilibrium,  $f$  and all its derivatives are zero, because the Jeans equation is satisfied. The second derivative of the Jeans equation,  $\partial^2 f / \partial x^2$ , which is related to the 3rd derivative of the gravitational potential, and, unlike the Jeans equation and its first derivative does not depend on the halo mass normalization, could serve as a metric for halo stability. Its usefulness in this capacity can be evaluated from the results of high resolution N-body simulations, by calculating it at different radii, and at different epochs during evolution. If  $\partial^2 f / \partial x^2$  proves to be a useful metric for stability, it can be employed in the search for possible dynamical attractors during the later stages of the collapse and relaxation of dark matter halos.

## 6 Acknowledgement

We would like to thank the anonymous referee for their insightful comments.

## References

- [1] J. E. Taylor and J. F. Navarro, *The Phase-Space Density Profiles of Cold Dark Matter Halos*, *ApJ* **563** (2001) 483 [[astro-ph/0104002](#)].
- [2] N. E. Drakos, J. E. Taylor and A. J. Benson, *The phase-space structure of tidally stripped haloes*, *MNRAS* **468** (2017) 2345 [[1703.07836](#)].
- [3] I. Butsky, A. V. Macciò, A. A. Dutton, L. Wang, A. Obreja, G. S. Stinson et al., *NIHAO project II: halo shape, phase-space density and velocity distribution of dark matter in galaxy formation simulations*, *MNRAS* **462** (2016) 663 [[1503.04814](#)].
- [4] C. Nolting, L. L. R. Williams, M. Boylan-Kolchin and J. Hjorth, *Testing DARKexp against energy and density distributions of Millennium-II halos*, *JCAP* **9** (2016) 042 [[1603.07337](#)].
- [5] L. Gao, J. F. Navarro, C. S. Frenk, A. Jenkins, V. Springel and S. D. M. White, *The Phoenix Project: the dark side of rich Galaxy clusters*, *MNRAS* **425** (2012) 2169 [[1201.1940](#)].

[6] A. D. Ludlow, J. F. Navarro, V. Springel, M. Vogelsberger, J. Wang, S. D. M. White et al., *Secondary infall and the pseudo-phase-space density profiles of cold dark matter haloes*, *MNRAS* **406** (2010) 137 [[1001.2310](#)].

[7] J. F. Navarro, A. Ludlow, V. Springel, J. Wang, M. Vogelsberger, S. D. M. White et al., *The diversity and similarity of simulated cold dark matter haloes*, *MNRAS* **402** (2010) 21 [[0810.1522](#)].

[8] C.-P. Ma, P. Chang and J. Zhang, *Is the Radial Profile of the Phase-Space Density of Dark Matter Halos a Power-Law?*, *arXiv e-prints* (2009) [[0907.3144](#)].

[9] S. R. Knollmann, A. Knebe and Y. Hoffman, *Phase-space density profiles in scale-free cosmologies*, *MNRAS* **391** (2008) 559 [[0809.1439](#)].

[10] Y. Hoffman, E. Romano-Díaz, I. Shlosman and C. Heller, *Evolution of the Phase-Space Density in Dark Matter Halos*, *ApJ* **671** (2007) 1108 [[0706.0006](#)].

[11] S. Peirani, F. Durier and J. A. de Freitas Pacheco, *Evolution of the phase-space density of dark matter haloes and mixing effects in merger events*, *MNRAS* **367** (2006) 1011 [[astro-ph/0512482](#)].

[12] C. G. Austin, L. L. R. Williams, E. I. Barnes, A. Babul and J. J. Dalcanton, *Semianalytical Dark Matter Halos and the Jeans Equation*, *ApJ* **634** (2005) 756 [[astro-ph/0506571](#)].

[13] K.-H. Chae, *A Universal Power-law Profile of Pseudo-phase-space Density-like Quantities in Elliptical Galaxies*, *ApJl* **788** (2014) L15 [[1311.1611](#)].

[14] E. Munari, A. Biviano and G. A. Mamon, *Mass, velocity anisotropy, and pseudo phase-space density profiles of Abell 2142*, *AAP* **566** (2014) A68 [[1311.1210](#)].

[15] C. Alard, *Dark matter haloes and self-similarity*, *MNRAS* **428** (2013) 340 [[1206.6548](#)].

[16] A. D. Ludlow, J. F. Navarro, S. D. M. White, M. Boylan-Kolchin, V. Springel, A. Jenkins et al., *The density and pseudo-phase-space density profiles of cold dark matter haloes*, *MNRAS* **415** (2011) 3895 [[1102.0002](#)].

[17] R. N. Henriksen, *Power Laws and Non-Power Laws in Dark Matter Halos*, *ApJ* **653** (2006) 894 [[astro-ph/0606654](#)].

[18] L. Bernaldo e Silva, W. de Siqueira Pedra and M. Valluri, *The Discreteness-driven Relaxation of Collisionless Gravitating Systems: Entropy Evolution and the Nyquist–Shannon Theorem*, *ApJ* **872** (2019) 20.

[19] A. Pontzen and F. Governato, *Conserved actions, maximum entropy and dark matter haloes*, *MNRAS* **430** (2013) 121 [[1210.1849](#)].

[20] E. Salvador-Solé, J. Viñas, A. Manrique and S. Serra, *Theoretical dark matter halo density profile*, *MNRAS* **423** (2012) 2190 [[1104.2334](#)].

[21] D.-B. Kang and P. He, *A statistical-mechanical explanation of dark matter halo properties*, *AAP* **526** (2011) A147 [[1012.1003](#)].

[22] P. He and D.-B. Kang, *Entropy principle and complementary second law of thermodynamics for self-gravitating systems*, *MNRAS* **406** (2010) 2678 [[0903.2208](#)].

[23] J. Hjorth and L. L. R. Williams, *Statistical Mechanics of Collisionless Orbits. I. Origin of Central Cusps in Dark-matter Halos*, *ApJ* **722** (2010) 851 [[1010.0265](#)].

[24] J. Hjorth, L. L. R. Williams, R. Wojtak and M. McLaughlin, *Non-universality of Dark-matter Halos: Cusps, Cores, and the Central Potential*, *ApJ* **811** (2015) 2 [[1508.02195](#)].

[25] L. L. R. Williams, J. Hjorth and R. Wojtak, *Statistical Mechanics of Collisionless Orbits. III. Comparison with N-body Simulations*, *ApJ* **725** (2010) 282 [[1010.0267](#)].

[26] L. J. Bernaldo e Silva, M. Lima and L. Sodré, *Testing phenomenological and theoretical models of dark matter density profiles with galaxy clusters*, *MNRAS* **436** (2013) 2616 [[1301.1684](#)].

[27] L. L. R. Williams and J. Hjorth, *Statistical Mechanics of Collisionless Orbits. II. Structure of Halos*, *ApJ* **722** (2010) 856 [[1010.0266](#)].

[28] A. Del Popolo, *On the pseudo phase-space density of dark matter haloes and the universality of density profiles*, *Baltic Astronomy* **24** (2015) 263.

[29] A. Del Popolo, *Non-power law behavior of the radial profile of phase-space density of halos*, *JCAP* **7** (2011) 014 [[1112.4185](#)].

[30] E. O. Nadler, S. P. Oh and S. Ji, *On the apparent power law in CDM halo pseudo-phase space density profiles*, *MNRAS* **470** (2017) 500 [[1701.01449](#)].

[31] E. Bertschinger, *Self-similar secondary infall and accretion in an Einstein-de Sitter universe*, *ApJs* **58** (1985) 39.

[32] S. H. Hansen and B. Moore, *A universal density slope Velocity anisotropy relation for relaxed structures*, *11* (2006) 333 [[astro-ph/0411473](#)].

[33] S. H. Hansen and J. Stadel, *The velocity anisotropy—density slope relation*, *JCAP* **5** (2006) 014 [[astro-ph/0510656](#)].

[34] D. Lemze, R. Wagner, Y. Rephaeli, S. Sadeh, M. L. Norman, R. Barkana et al., *Profiles of Dark Matter Velocity Anisotropy in Simulated Clusters*, *ApJ* **752** (2012) 141 [[1106.6048](#)].

[35] S. H. Hansen and R. Piffaretti, *Measuring the dark matter velocity anisotropy in galaxy clusters*, *AAP* **476** (2007) L37 [[0705.4680](#)].

[36] S. H. Hansen, A. V. Macciò, E. Romano-Díaz, Y. Hoffman, M. Brüggen, E. Scannapieco et al., *The Temperature of Hot Gas in Galaxies and Clusters: Baryons Dancing to the Tune of Dark Matter*, *ApJ* **734** (2011) 62 [[1012.2870](#)].

[37] A. Longobardi, M. Arnaboldi, O. Gerhard, C. Pulsoni and I. Söldner-Rembold, *Kinematics of the outer halo of M 87 as mapped by planetary nebulae\**, *AAP* **620** (2018) A111 [[1809.10708](#)].

[38] E. Vasiliev, *Proper motions and dynamics of the Milky Way globular cluster system from Gaia DR2*, *MNRAS* **484** (2019) 2832 [[1807.09775](#)].

[39] L. L. R. Williams, C. Austin, E. Barnes, A. Babul and J. Dalcanton, *The Phase-space Density Distribution of Dark Matter Halos*, in *Baryons in Dark Matter Halos*, R. Dettmar, U. Klein and P. Salucci, eds., p. 20, Dec., 2004, [astro-ph/0412442](#).

[40] E. I. Barnes, L. L. R. Williams, A. Babul and J. J. Dalcanton, *Density Profiles of Collisionless Equilibria. II. Anisotropic Spherical Systems*, *ApJ* **654** (2007) 814 [[astro-ph/0609784](#)].

[41] J. Einasto, *On the Construction of a Composite Model for the Galaxy and on the Determination of the System of Galactic Parameters*, *Trudy Astrofizicheskogo Instituta Alma-Ata* **5** (1965) 87.

[42] J. F. Navarro, E. Hayashi, C. Power, A. R. Jenkins, C. S. Frenk, S. D. M. White et al., *The inner structure of  $\Lambda$ CDM haloes - III. Universality and asymptotic slopes*, *MNRAS* **349** (2004) 1039 [[astro-ph/0311231](#)].

## A Finite difference integration of Jeans Equation

The RHS of eq. (3.1) is totally independent of any derivatives and the mass of a DM halos is calculated as a function of radius by numerically integrating  $\rho$  with increasing radius.

$$M(x) = \int_0^x 4\pi x^2 \rho(x) dx = \sum_{x=0}^r 4\pi x^2 \rho(x) \Delta x \quad (\text{A.1})$$

where  $\Delta x$  is the step size used for the summation. We solve the differential eq. (3.1) by integration it on both sides and converting the integral to a summation

$$\frac{\rho(x)\sigma^2(x)}{3 - 2\beta(x)} + \sum_{x=0}^r \frac{2\beta(x)}{3 - 2\beta(x)} \frac{\rho(x)\sigma^2(x)}{x} \Delta x = - \sum_{x=0}^r G\rho(x) \frac{M(x)}{x^2} \Delta x \quad (\text{A.2})$$

Now using the finite difference method and applying the backward difference with the assumption that eq. (A.2) is true at all the steps in the radii, we approximate the solution for  $\sigma^2$  as :

$$\frac{\rho(x)\sigma^2(x)}{3 - 2\beta(x)} - \frac{\rho(x - \Delta x)\sigma^2(x - \Delta x)}{3 - 2\beta(x - \Delta x)} + \frac{2\beta(x)}{3 - 2\beta(x)} \frac{\rho(x)\sigma^2(x)}{x} \Delta x = -\rho(x) \frac{M(x)}{x^2} \Delta x \quad (\text{A.3})$$

using the boundary conditions,  $\sigma$  profile for a particular parameter set at all radii is computed.